Journal of Solid State Chemistry 307 (2022) 122832

Contents lists available at ScienceDirect

Journal of Solid State Chemistry

journal homepage: www.elsevier.com/locate/jssc

Structural, thermal and electrical studies of thallium-scandium-hafnium(zirconium) molybdates

Victoria G. Grossman [a,*], Maxim S. Molokeev [b,c], Jibzema G. Bazarova [a], Bair G. Bazarov [a], Nikolay I. Sorokin [d]

[a] Baikal Institute for Nature Management, SB RAS, Sakhyanovoy St. 6, Ulan-Ude, 670047, Russia
[b] Kirensky Institute of Physics, Federal Research Center KSC, Siberian Branch, Academy of Sciences, 50 / 38 Akademgorodok, Krasnoyarsk, 660036, Russia
[c] Research and Development Department, Kemerovo State University, Kemerovo, 650000, Russia
[d] Shubnikov Institute of Crystallography, Federal Scientific Research Centre "Crystallography and Photonics," Russian Academy of Sciences, Moscow, 119333, Russia

ARTICLE INFO

Keywords:
Synthesis
Scandium
Thallium
Molybdates
Impedance spectroscopy
Conducting material

ABSTRACT

Thallium scandium hafnium molybdate $Tl_5ScHf(MoO_4)_6$ and thallium scandium zirconium molybdate $Tl_5ScZr(MoO_4)_6$ crystallize in trigonal symmetry with the space group $R\bar{3}c$. The compounds are synthesized by sintering the finely powdered simple molybdates mixture in a muffle furnace at 723–823 K for 100 h. The crystal structures of $Tl_5ScHf(MoO_4)_6$ and $Tl_5ScZr(MoO_4)_6$ are obtained by Rietveld method. The following unit cell parameters are calculated for $Tl_5ScHf(MoO_4)_6$: $a = 10.62338$ (5), $c = 38.0579$ (2) Å, $V = 3719.64$ (4) Å^3, $Z = 6$ and for $Tl_5ScZr(MoO_4)_6$: $a = 10.63216$ (7), $c = 38.0716$ (3) Å, $V = 3727.14$ (5) Å^3, $Z = 6$. The conductivity of the $Tl_5ScHf(MoO_4)_6$ and $Tl_5ScZr(MoO_4)_6$ are measured between 293 and 860 K. The ionic conductivity of $Tl_5ScHf(MoO_4)_6$ and $Tl_5ScZr(MoO_4)_6$ molybdates are 8×10^{-4} S/cm and 8×10^{-3} S/cm (at 773 K); the activation energy of ionic transfer are 0.8 eV and 0.3 eV respectively.

1. Introduction

At present, a fairly large number of molybdates with both a layered structure and a framework structure are known. Molybdates of various structural families have a number of useful properties. For example, electric, magnetic, laser materials, good optical and catalytic properties [1–20]. Among complex molybdates of interest, lyonsite-structure such as $NaCo_{2.31}(MoO_4)_{3.5}$ [21], $Na_2Co_2(MoO_4)_3$ [22], $Li_3Fe(MoO_4)_3$ [23], $Li_2Co_{2-x}Ni_x(MoO_4)_3$ ($0 \le x \le 2$) [24], $Na_{0.24}Ti_{1.44}(MoO_4)_3$ [25], Nasicon structure such as $Na_{2x}M_2Sc_{2(1-x)}(MoO_4)_3$ where M = Zn, Cd and Mg [26], alluaudite-type such as $Na_5In(MoO_4)_4$ [27], $Na_{25}Cs_8R_5(MoO_4)_{24}$ (R = In, Sc, Fe) [28], $K_{0.13}Na_{3.87}Mg(MoO_4)_3$ [29] are described.

Complex oxides based on alkali earth, trivalent metals, and 4d, 5d-transition metals (Mo, Hf) with the NASICON-type structure attract significant attention due to high-ionic conductivity. Indeed, the ionic conductivity reaches 10^{-3}–10^{-1} S/cm for the NASICON-type molybdates $Na_3Sc(MoO_4)_3$, $Cs_2Zr(MoO_4)_3$ [30], $Ag_{1-x}Mg_{1-x}R_{1+x}(MoO_4)_3$ (R = Al or Sc and $0 \le x \le 0.5$) [31], $Na_{1-x}Co_{1-x}Sc_{1+x}(MoO_4)_3$, $0 \le x \le 0.5$ [32], $Na_{1-x}Ni_{1-x}Sc_{1+x}(MoO_4)_3$, $0 \le x \le 0.5$ [33], $Na_{1-x}Co_{1-x}Fe_{1+x}(MoO_4)_3$, $0 \le x \le 0.4$ [34], $Li_{0.2}K_{0.8-y}Mg_{1-x}Sc(Lu)_{1+x}(MoO_4)_3$ ($0 \le x \le 0.5$, $0 \le y \le 0.3$) [35]. In recent years, NASICON-like compounds with the general formula $A_5RM(MoO_4)_6$, where A^+ are monovalent ions, R^{3+} are trivalent, and M^{4+} are tetravalent cations [36–44] are very intensively studied.

In these compounds, the framework is constructed of MoO_4 tetrahedra linked to the $(R,M)O_6$ octahedra by corner sharing, due to which channels for fast ion transport are formed, and also leads to a large variety of crystal structures with a high capacity for cationic and anionic substitutions.

Currently, very few works are devoted to the study of molybdates, where thallium is used as the monovalent cation [45–49]. For example, the ternary systems Tl_2MoO_4–$R_2(MoO_4)_3$–$Hf(MoO_4)_2$ (R = In, Bi) [47,48] were studied, the $Tl_5RHf(MoO_4)_6$ (R = In, Bi) phases were found, which crystallize in the space group $R\bar{3}c$. It was found that in the systems Tl_2MoO_4–$R_2(MoO_4)_3$–$Hf(MoO_4)_2$ (R = Cr, Fe) [46,49] are formed molybdates of two compositions $Tl_5RHf(MoO_4)_6$ (R = Cr, Fe) and $TlRHf_{0.5}(MoO_4)_3$ (R = Cr, Fe). Triple molybdates were prepared of the solid-state reaction method using the mixtures of stoichiometric amounts of simple molybdates, and also their electrical properties were studied. The thallium-chromium-hafnium molybdate showed rather high values of conductivity ($\sigma = 1.2 \times 10^{-2}$ S/cm at 773 K) [49].

* Corresponding author.
E-mail address: grossmanv@mail.ru (V.G. Grossman).

https://doi.org/10.1016/j.jssc.2021.122832
Received 7 September 2021; Received in revised form 12 December 2021; Accepted 15 December 2021
Available online 18 December 2021

Thereby we set the task to improve the ion-conducting properties of the obtained $Tl_5CrHf(MoO_4)_6$ by replacing chromium with scandium and hafnium with zirconium.

2. Experimental

2.1. Characterization methods

PXRD patterns were recorded on a Bruker D8 ADVANCE X-ray diffractometer (Bruker, Berlin, Germany) with Cu-K_α radiation (λ = 1.5418 Å) at room temperature. The scanning range is between 5 and 100° with a scanning width of 0.02 and a rate of 0.1 s^{-1}.

The variable counting time (VCT) scheme was used to collect the diffraction data. The VCT data were used to refine the structures by the Rietveld method. The measurement time was systematically increased towards higher 2θ angles, leading to drastically improved data quality [50,51]. To collect the X-ray data using VCT scheme, five ranges were generated on the diffraction pattern: 8°–32.0° (exposure per point: 0.5 s; step: 0.0069°), 32.0°–59.0° (exposure per point: 1 s; step: 0.0069°), 59.0°–86.0° (exposure per point: 2 s; step: 0.0069°), 86.0°–113.0° (exposure per point: 4 s; step: 0.0069°) and 113.0°–130° (exposure per point: 8 s; step: 0.0069°). Total experimental time was equal to ~19 h. The esd's σ(I_i) of all points on patterns were calculated using intensities I_i: $\sigma(I_i) = I_i^{1/2}$. The intensities and obtained esd's were further normalized, taking into account actual value of exposition time, and saved in xye-type file. So transformed powder pattern has usual view in whole 2θ range 8–130°, but all high-angle points have small esd's.

The thermal gravity-differential scanning calorimetric (TG-DSC) analyses of $Tl_5ScHf(MoO_4)_6$ and $Tl_5ScZr(MoO_4)_6$ were performed on a NETZSCH STA 449 F1 thermal analyzer instrument. Thermal measurements were carried out on samples placed in a platinum crucible. The samples charge was 17–18 mg, and the rate of temperature rise was 10 K/min under the Ar atmosphere. The DSC curves were calculated using a standard developed program from Netzsch.

Impedance spectroscopy measurements were carried out using a *Z*-1500*J* impedance meter. The impedance spectra were recorded in the 1 Hz−1 MHz frequency range. Ceramic pellets for dielectric investigations were prepared by isostatic pressing at 100 bar and sintering at 773 K for 1 and 3 h in air with 10 K/min heating and cooling rates. The resulting disks had a diameter of 10 mm and a thickness of 1–2 mm. For the making of electrodes, large surfaces of the disks were covered with a paste, which was a mixture of hexachloroplatinate (IV) ammonium $(NH_4)_2[PtCl_6]$ in toluene. Then, the tablet with the applied paste was annealed at a temperature of about 773 K for 1 h. The total electrical conductivity σ_{tot} for each temperature was calculated from:

$$\sigma_{tot} = L/(R_{tot} \times S). \quad (1)$$

where R_{tot} is the total conductivity, L is the thickness of specimen, and S is the area of round surface.

The activation energy for ionic conduction E_a was found from the Arrhenius–Frenkel equation

$$\sigma_{tot}T = A\exp(-E_a/kT), \quad (2)$$

where A is the preexponential factor of the electrical conductivity, k is the Boltzmann constant, and T is temperature.

The experimental-to-*X*-ray density ratio was used as the criterion for evaluation of the density of the resulting ceramics. The experimental density was calculated by dividing the weight of the sintered sample by its volume estimated from geometric dimensions. The size was measured with an accuracy of ±0.01 mm. The *X*-ray density of molybdates was calculated by the equation,

$$\rho_X = 1.66MZ/V, \quad (3)$$

where M is the molecular weight of the formula unit of a substance, Z is the number of formula units, and V is the unit cell volume.

2.2. Preparation of samples

$Tl_5ScHf(MoO_4)_6$ and $Tl_5ScZr(MoO_4)_6$ in the form of powders were prepared by solid-state reactions between stoichiometric amounts of presynthesized Tl_2MoO_4, $Sc_2(MoO_4)_3$, $Hf(MoO_4)_2$ and $Zr(MoO_4)_2$ at 723–823 K for 100 h.

We obtained the thallium molybdate from Tl_2CO_3 (chemically pure, Red Chemist, Russia) and MoO_3 (chemically pure, Red Chemist, Russia) by the following reaction:

$$Tl_2CO_3 + MoO_3 = Tl_2MoO_4 + CO_2$$

at 673–823 K for 100 h. Zirconium and hafnium molybdates were synthesized by reacting stoichiometric mixtures of $ZrO(NO_3)_2\ H_2O$ (chemically pure, IGIC RAS, Russia), HfO_2 (chemically pure, IGIC RAS, Russia), and MoO_3 at 673–1023 K for 100 h. The starting reagents were well mixed and ground in an agate mortar with a pestle. Due to the fact that molybdenum oxide sublimes below the melting point, the synthesis of simple molybdates was beginning at a temperature of 673 K.

A stoichiometric mixture of $Sc(NO_3)_3$ (Joint Stock Company Kiev Plant of Reagents, Indicators and Analytical Products « RIAP») and MoO_3 was used for the synthesis of simple molybdate $Sc_2(MoO_4)_3$ in the temperature range 623–1073 K for 100 h. The annealing was started at a temperature of 623 K to avoid the release of reagents due to the violent evolution of nitrogen oxide and oxygen. To accelerate the interaction, the reaction mixtures were gradually annealed at the temperatures specified in the interval and ground after every 24 h of annealing.

3. Results and discussion

3.1. Structural study

Rietveld refinements were performed by using TOPAS 4.2 [52] which accounts esd's of each point by special weight scheme. All peaks, besides small impurity peaks in $Tl_5ScZr(MoO_4)_6$ compound, were indexed by trigonal cell (sp. gr. $R\bar{3}c$) with parameters close to $K_5InHf(MoO_4)_6$ [53]. Therefore, this structure was taken as starting model for refinement. Refinement was stable and gave low *R*-factors (Table 1, Fig. 1). Coordinates of atoms and main bond lengths are in Tables 1S and 2S respectively. The K^+ ion was replaced by Tl^+. Two Hf^{4+}/In^{3+} sites were occupied by Hf^{4+}/Sc^{3+} ions and Zr^{4+}/Sc^{3+} ions for $Tl_5ScHf(MoO_4)_6$ and $Tl_5ScZr(MoO_4)_6$, respectively (Fig. 2). The Hf^{4+}/Sc^{3+} and Zr^{4+}/Sc^{3+} occupancies were refined taking into account that sum of occupancies is equal to 1 in each site. In order to reduce number of refined parameters, only one thermal parameter was refined for all oxygen atoms.

The crystallographic data are deposited in Cambridge Crystallographic Data Centre (CCDC # 2103627–2103628). The data can be downloaded from the site (www.ccdc.cam.ac.uk/data_request/cif).

3.2. Thermal analysis

The thermal analysis curves of $Tl_5ScHf(MoO_4)_6$ and $Tl_5ScZr(MoO_4)_6$

Table 1
Main parameters of processing and refinement of the $Tl_5ScHf(MoO_4)_6$ sample.

Compound	$Tl_5ScHf(MoO_4)_6$	$Tl_5ScZr(MoO_4)_6$
Sp.Gr.	$R\bar{3}c$	$R\bar{3}c$
a, Å	10.62338 (5)	10.63216 (7)
c, Å	38.0579 (2)	38.0716 (3)
V, Å^3	3719.64 (4)	3727.14 (5)
Z	6	6
2*θ*-interval, °	8–130	8–130
R_{wp}, %	4.47	5.47
R_p, %	4.81	6.28
R_{exp}, %	3.14	3.02
χ^2	1.42	1.81
R_B, %	2.16	5.47

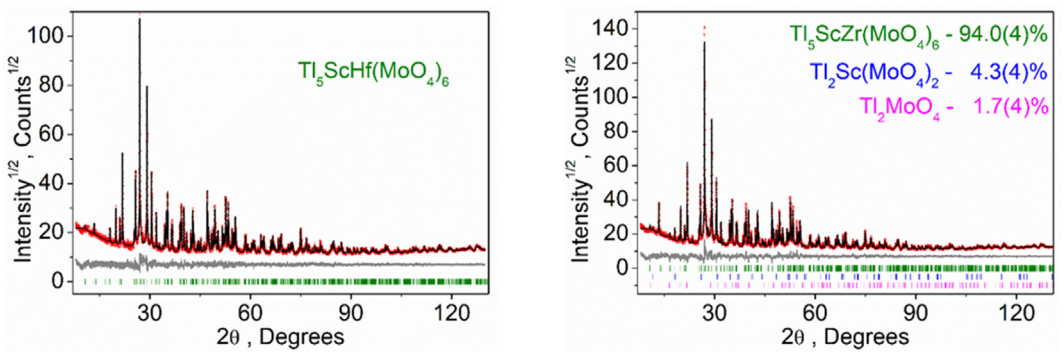

Fig. 1. Difference Rietveld plots of (a) $Tl_5ScHf(MoO_4)_6$ and (b) $Tl_5ScZr(MoO_4)_6$.

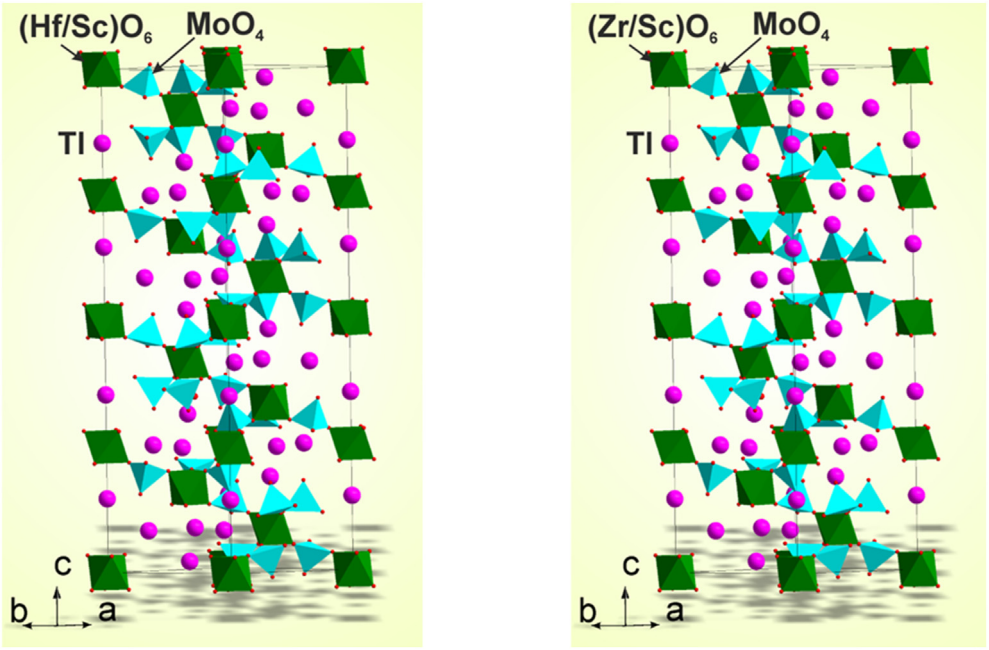

Fig. 2. Crystal structure of (a) $Tl_5ScHf(MoO_4)_6$ and (b) $Tl_5ScZr(MoO_4)_6$.

performed in the thermal range from room temperature to ~950 K are shown in Fig. 3 and Fig. 4. The very minor weight loss, on the order of 1%, can be attributed associated with the evaporation of a small amount of surface moisture. The endothermic effect started at 906 K ($\Delta H = -80420.28$ J/mol) is due to melting of $Tl_5ScHf(MoO_4)_6$ molybdate and at 890 K ($\Delta H = -92401.44$ J/mol) due to melting of $Tl_5ScZr(MoO_4)_6$ (blue curve). While cooling the sample (red curve), one exothermic peak is

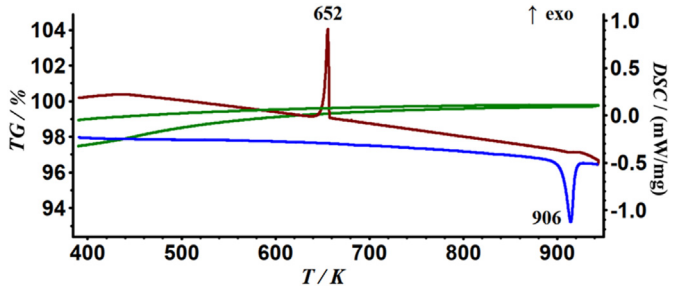

Fig. 3. DSC and TG curves of the $Tl_5ScHf(MoO_4)_6$. The green curve is TG curve, the blue curve is heating, the red curve is cooling. (For interpretation of the references to colour in this figure legend, the reader is referred to the Web version of this article.)

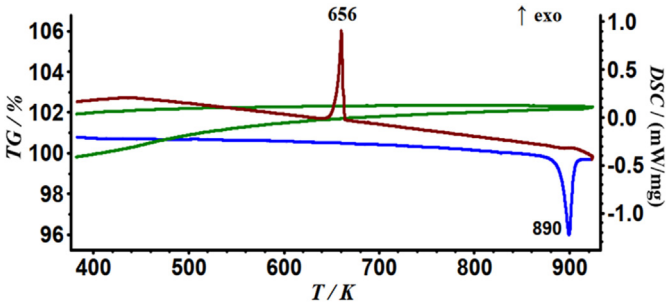

Fig. 4. DSC and TG curves of the $Tl_5ScZr(MoO_4)_6$. The green curve is TG curve, the blue curve DSC is heating, the red curve DSC is cooling. (For interpretation of the references to colour in this figure legend, the reader is referred to the Web version of this article.)

observed at 652 K ($\Delta H = 54730.78$ J/mol) for $Tl_5ScHf(MoO_4)_6$ and at 656 K ($\Delta H = 68046.26$ J/mol) for $Tl_5ScZr(MoO_4)_6$.

3.3. Electrical properties

Electrical measurements were performed by the impedance

spectroscopy technique at frequencies from 1 Hz to 1 MHz in an electrochemical cell with platinum electrodes. Impedance plots of polycrystalline solid electrolytes typically have the form of a combination of three elements associated with capacitance values in the range of picofarad per centimeter, nanofarad per centimeter and microfarad per centimeter corresponding to grain interior (bulk), grain boundary (internal interfaces) and electrode processes (material/electrode interfaces), respectively.

$Tl_5ScHf(MoO_4)_6$ monophasic powder pellets were sintered at a temperature of 773 K for 1 and 3 h, followed by measurement of the density of the pellets and electrical characteristics.

As a result of sintering at 773 K for 1 h, a pellet density of 83% of theoretical was achieved. When increasing the duration of annealing of the pellets up to 3 h, their density practically did not increase. Figs. 5 and 6 show a set of impedance data $Z^*(\omega) = Z' + iZ''$ of $Tl_5ScHf(MoO_4)_6$ and $Tl_5ScZr(MoO_4)_6$ taken over a wide frequency range at different temperatures as a Nyquist diagram (complex impedance spectrum). The capacitance values estimated experimentally from deformed semicircles using the equation $C = 1/2\pi f_{max}Z$, where f_{max} is frequency of the peak maxima, have values of 10^{-10} F, which can be considered as the average values of the capacitances for bulk and grain boundary conductivity (10^{-12} and 10^{-8} F). In this regard, it was not possible to separate the grain and the grain boundary contribution the Nyquist diagram (Fig. 5a–b).

Thus, the semicircle in the $-Z''$ vs. Z' plots is associated with the sum of both contributions. As the impedance decreases with temperature, the total electrical conductivity of the prepared ceramics shows an increase with the increase in temperature. It can be seen in Fig. 5a–b that an increase in the nucleation time leads to a decrease in the R_{tot} resistivity,

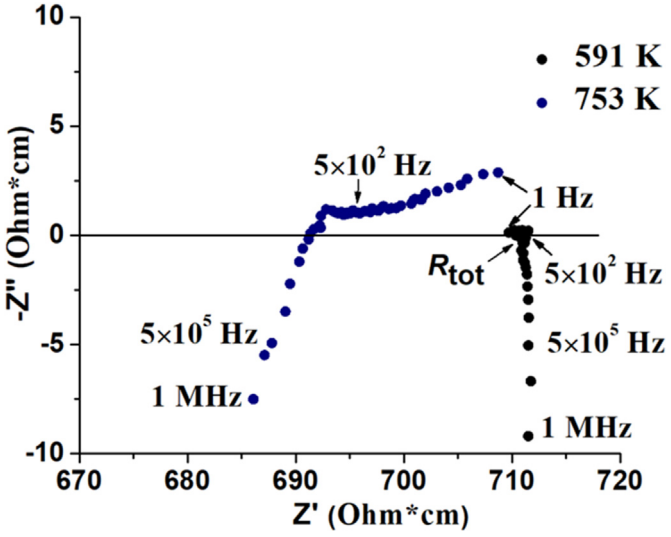

Fig. 6. Impedance spectra of $Tl_5ScZr(MoO_4)_6$.

read at the low-frequency intersection of the impedance semicircle with the Z' axis. This indicates a decrease of the barrier to the mobility of charge carriers, which contribute to electrical conductivity. The presence of a low-frequency spur indicates that the electrical conductivity of the $Tl_5ScHf(MoO_4)_6$ sample is inherently ionic. This behavior is in good agreement with the results reported in our previous works on the $Tl_5RHf(MoO_4)_6$ (R = Cr, In, Bi) [47–49].

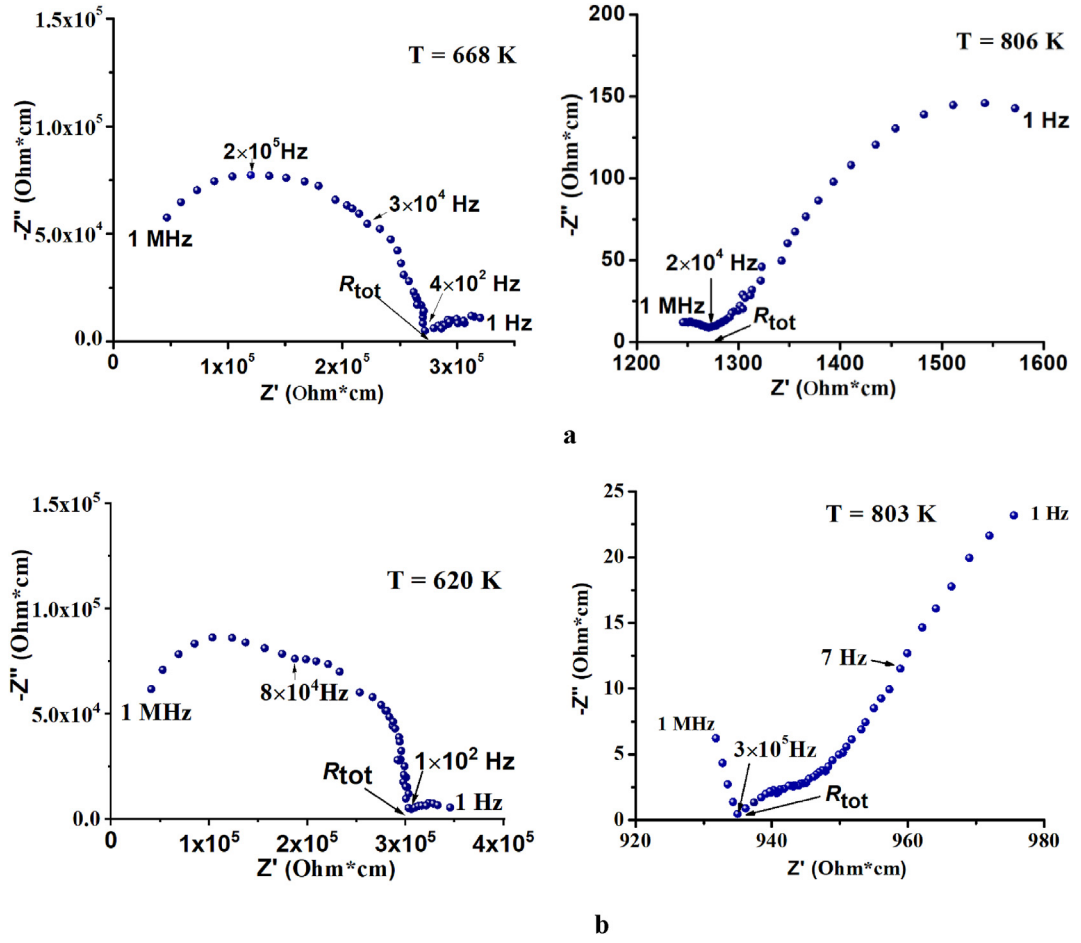

Fig. 5. Impedance spectra of $Tl_5ScHf(MoO_4)_6$ pellet synthesized within 1 h (a) and 3 h (b) at 773 K.

The resistance values of total (R_{tot}) of the ceramic pellets were taken from the intercepts of semicircles on Z'-axis and then converted into corresponding conductivities σ_{tot}. The variations of conductivities σ_{tot} with temperature for $Tl_5ScHf(MoO_4)_6$ and $Tl_5ScZr(MoO_4)_6$ are represented as Arrhenius plots in the 623–860 K (for pellet of $Tl_5ScHf(MoO_4)_6$ synthesized within 1 h, Fig. 7a), 622–810 K (for pellet of $Tl_5ScHf(MoO_4)_6$ synthesized within 3 h, Fig. 7b) and 650–823 K for pellet $Tl_5ScZr(MoO_4)_6$ (Fig. 8). All the dependencies have two linear parts with different slopes. A change in the slope is observed near the temperature of transition.

Both below and above the phase transition, the dependences are adequately described by the Arrhenius–Frenkel law; i.e., the observed processes are thermally activated. The activation energies of conductivity in the temperature region above the phase transition point (795–834 K, cooling mode for pellet synthesized within 1 h) is estimated to be E_a = 0.80 eV ($A = 7.2 \times 10^4$ SK/cm). The activation energy of conductivity for a tablet synthesized for 3 h, in heating mode at 749–813 K and cooling mode at 717–803 K, is estimated to be E_a = 0.79 eV (A = 8.3×10^4 SK/cm).

If we assume, based on the DSC data, that melting and the solid-state transition are the thermal effects for the studied molybdates, we can calculate the entropy of fusion S_m and the entropies of the solid-state transition S_{tr} and compare them. Then, according to the work of C.E. Derrington et al. [54] in the case of closeness or comparability of the entropies of S_m and S_{tr}, this indicates a strong disorder and high ionic conductivity of one of the sublattices in the high-temperature state of the crystal after the phase transition. For the studied molybdates, the indicated sublattice is the thallium sublattice. Let us check this assumption for $Tl_5ScHf(MoO_4)_6$ molybdate: $S_m = H_m/T_m$ = 88.76 J/(mol·K) and $S_{tr} = H_{tr}/T_{tr}$ = 83.94 J/(mol·K). The values of the entropy of fusion S_m and the entropy of the solid-state transition S_{tr} are close. The situation is similar for $Tl_5ScZr(MoO_4)_6$ molybdate: S_m = 103.82 J/(mol·K) and S_{tr} = 103.72 J/(mol·K).

Fig. 7b shows that with an increase in the nucleation time leads up to 3 h, the conductivity did not change, but at the same time, the area of the region that appeared when crossing the conductivity curves obtained by heating and cooling molybdate Fig. 7b shows that with an increase in the nucleation time leads up to 3 h, the conductivity did not change, but at the same time, the area of the region that appeared when crossing the conductivity curve obtained by heating and cooling molybdate decreased. Molybdate $Tl_5ScHf(MoO_4)_6$ has a low conductivity (~10^{-7} S/cm at 500 K), as a result of a phase transition it passes into the superionic state (~10^{-3} S/cm at 800 K). In the high-temperature range (717–803 K) the activation energy for electrical conduction is ~0.8 eV and the electrical conductivity reaches 8×10^{-4} S/cm at 773 K. These data coincide with the parameters of Tl^+ ions transport in the high-temperature (775–820 K) modification of $Tl_5InHf(MoO_4)_6$ [47]: $\sigma = 7 \times 10^{-4}$ S/cm at 773 K and E_a = 0.85 eV.

In Fig. 8, upon heating, the curve σ_{tot}(T) first shows a section with electronic conductivity (with increasing temperature, the value of σ_{tot} decreases) in the temperature range of 620–715 K. Further, a transition region is observed between sections with ionic and electronic conductivity at 715–740 K, which falls into the phase transition region. The phase transition begins at 740 K and practically ends at a measured maximum temperature of about 820 K.

In the temperature range 740–820 K (cooling mode) the activation energy for conduction is ~0.3 eV and the electrical conductivity reaches 8×10^{-3} S/cm at 773 K. The electrical conductivity value of the $Tl_5ScZr(MoO_4)_6$ sample is ~10 times larger than the conductivity of $Tl_5ScHf(MoO_4)_6$, but is inferior to $Tl_5CrHf(MoO_4)_6$ (1.2×10^{-2} S/cm [49]). The value of E_a for $Tl_5ScZr(MoO_4)_6$ is significantly lower than the activation energy for electrotransfer in $Tl_5ScHf(MoO_4)_6$ (0.8 eV). The reason for the low E_a for $Tl_5ScZr(MoO_4)_6$ molybdate requires additional research; possibly, this is due to the influence of the electronic subsystem on the characteristics of ion transfer.

The crystal-chemical analysis of $Tl_5Sc\mathit{M}(MoO_4)_6$ (M = Hf/Zr) compounds shows that the multiply charged Sc^{3+}, Hf^{4+}/Zr^{4+}, Mo^{6+} cations,

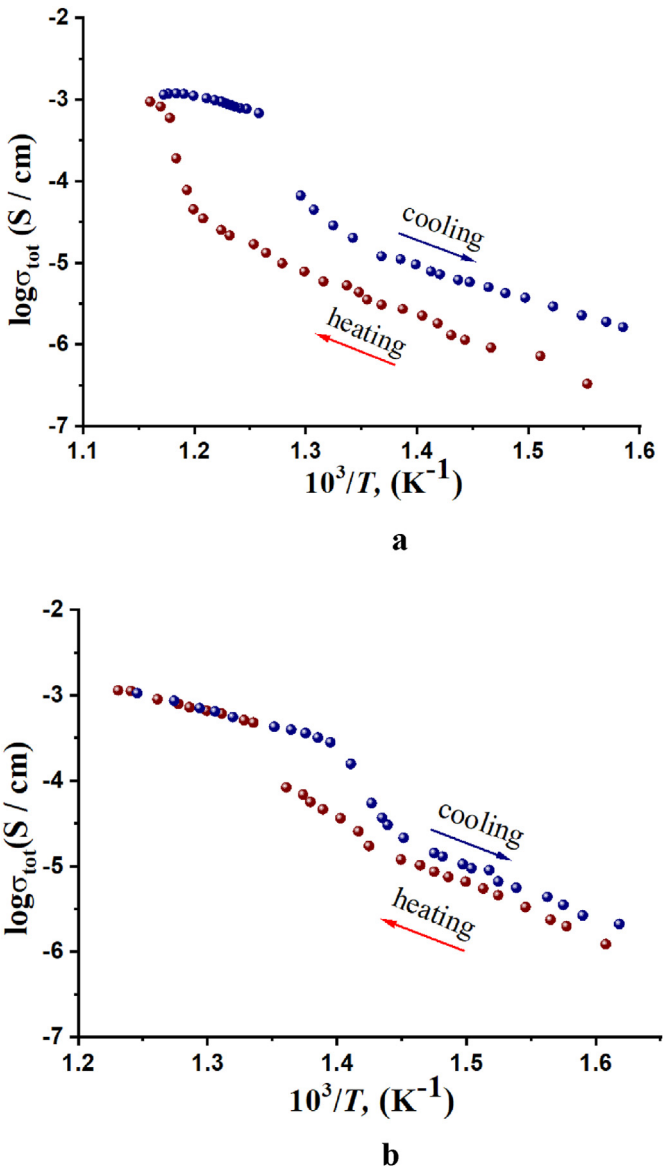

Fig. 7. Dependence of the total conductivity of $Tl_5ScHf(MoO_4)_6$ pellet synthesized within 1 h (a) and 3 h (b) on temperature.

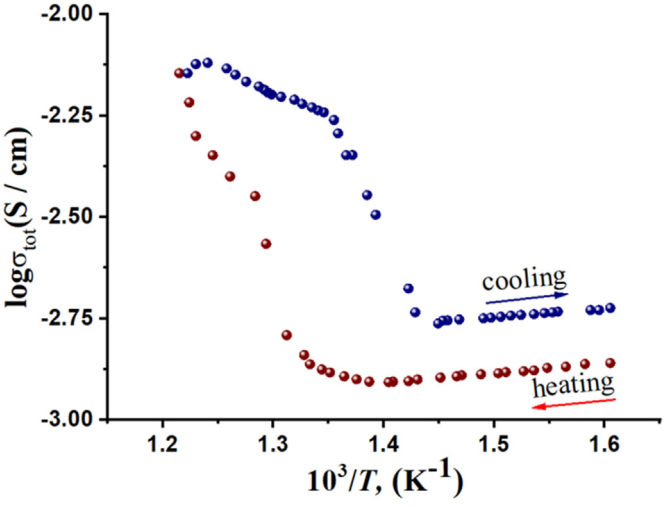

Fig. 8. Dependence of the total conductivity of $Tl_5ScZr(MoO_4)_6$ on temperature.

Table 2
Electrophysical properties of isostructural ternary molybdates $Tl_5RM(MoO_4)_6$ (R = Sc, In, Bi, Cr; M = Hf, Zr).

Molybdate	Conductivity, S/cm at 773 K	The activation energy of electrotransfer, eV	Ref.
$Tl_5ScHf(MoO_4)_6$	8×10^{-4}	0.8 (715–810 K)	this
$Tl_5ScZr(MoO_4)_6$	7×10^{-3}	0.3 (740–830 K)	study
$Tl_5InHf(MoO_4)_6$	7×10^{-4}	0.85 (775–820 K)	[47]
$Tl_5BiHf(MoO_4)_6$	2×10^{-6}	1.4 (675–770 K)	[48]
$Tl_5CrHf(MoO_4)_6$	1.2×10^{-2}		[49]

which are part of the crystal framework, form stronger chemical bonds with oxygen than singly charged Tl^+ cations located in structural channels. This indicates higher mobility of Tl^+ cations in comparison with the "framework" cations Sc^{3+}, Hf^{4+}/Zr^{4+}, Mo^{6+}. In the three-dimensional crystal framework, one can select a channel of internal voids containing Tl^+ ions, which compensate for the negative framework charge. Tl^+ cations have an anomalously large vibration amplitude (Table 1S) and interact electrostatically with the negatively charged framework, which indicates their high mobility. Weak bonding of Tl^+ ions with the framework induces the occurrence of ionic conductivity.

The mobility of thallium ions for an isostructural compound $Tl_{4.86}Fe_{0.82}Hf_{1.18}(MoO_4)_6$was confirmed by us in our work [46]. We were established structure and possible thallium ion-transport paths analyzed based on the calculated total probability density function. An analysis of the possible thallium ion-transport paths and an estimation of the height of the potential barrier showed that the ion current is most likely in the *ab* plane.

Table 2 shows the electrical conductivity characteristics for some isostructural (sp. gr. $R\bar{3}c$) ternary molybdates $Tl_5RM(MoO_4)_6$. As can be seen from Table 2, the electrophysical characteristics of $Tl_5CrHf(MoO_4)_6$ molybdate do not improve when Cr^{3+} is replaced by Sc^{3+} and Hf^{4+} by Zr^{4+}. However, the nature of the cations included in the rigid framework has a noticeable effect on the ionic conductivity of complex molybdates with a framework structure. Therefore, it is necessary to continue the search for Tl^+-ionic conductors, especially in the region of low temperatures (300–500 K).

Recently, a whole set of studies has been conducted to study the structural, thermal, and electrical properties of ternary thallium molybdates [45–49,55]. Due to the wide possibilities of varying the elemental and quantitative compositions, ternary thallium molybdates are convenient model objects for the solid-state chemistry and establishing genetic "composition – structure – properties" relationships.

4. Conclusion

The geometrical sizes of Tl^+ cations (r_i = 1.50 Å [56]) significantly exceed the sizes of Li^+ (r_i = 0.76 Å) and Na^+ (r_i = 1.02 Å); therefore, for their migration, the crystal structures must have wide overlapping conduction channels. Few of such crystal structures are known. These include "loose" framework structures of $Tl_5ScM(MoO_4)_6$ compounds with M = Hf and Zr. The rigid framework of $Tl_5ScM(MoO_4)_6$ molybdates is formed by MoO_4 tetrahedra and (Sc, Hf/Zr)O_6 octahedra linked by common oxygen vertices (Fig. 2). In large cavities of the framework, mobile Tl^+ cations are located in two crystallographic positions. The high mobility of Tl^+ cations is indicated by the fact that their vibration amplitude in structural positions (B_{iso}, Table 1S) is much higher than for other ions. It follows from the crystal-chemical analysis that it is precisely the Tl^+ cations that are ionic carriers in the ternary molybdates $Tl_5ScM(MoO_4)_6$ (M = Hf, Zr).

CRediT authorship contribution statement

Victoria G. Grossman: Investigation, Writing – original draft, preparation, Writing – review & editing. **Maxim S. Molokeev:** Writing – original draft, preparation, Writing – review & editing, Refinement of the structure by the Rietveld method and co-wrote the paper. **Jibzema G. Bazarova:** Conceptualization. **Bair G. Bazarov:** Resources. **Nikolay I. Sorokin:** Writing – original draft, preparation, Writing – review & editing.

Declaration of competing interest

The authors declare that they have no known competing financial interests or personal relationships that could have appeared to influence the work reported in this paper.

Acknowledgments

The work was supported by Basic Project of BINM SB RAS №0273-2021-0008. Research was conducted using equipment of the CCU BINM SB RAS. Structural analysis of materials in this study was partly supported by the Research Grant No. 075-15-2019-1886 from the Government of the Russian Federation.

Appendix A. Supplementary data

Supplementary data to this article can be found online at https://doi.org/10.1016/j.jssc.2021.122832.

References

[1] L. Balsanova, D. Mikhailova, A. Senyshyn, D. Trots, H. Fuess, W. Lottermoser, H. Ehrenberg, Structure and properties of α-$AgFe_2(MoO_4)_3$, Solid State Sci. 11 (2009) 1137–1143, https://doi.org/10.1016/j.solidstatesciences.2009.03.006.
[2] R. Ishii, S. Tanaka, K. Onuma, Y. Nambu, M. Tokunaga, T. Sakakibara, N. Kawashima, Y. Maeno, C. Broholm, D.P. Gautreaux, J.Y. Chan, S. Nakatsuji, Successive phase transitions and phase diagrams for the quasi-two-dimensional easy-axis triangular antiferromagnet $Rb_4Mn(MoO_4)_3$, Europhys. Lett. 94 (2011) 17001–17006.
[3] D. Mikhailova, A. Sarapulova, A. Voss, A. Thomas, S. Oswald, W. Gruner, D.M. Trots, N.N. Bramnik, $Li_3V(MoO_4)_3$: a new material for both Li extraction and insertion, Chem. Mater. 22 (2010) 3165–3173, https://doi.org/10.1021/cm100213a.
[4] M. Mhiri, A. Badri, M.L. Lopez, C. Pico, M. Ben Amara, Synthesis, crystal structure, magnetic properties and ionic conductivity of $NaMFe(MoO_4)_3$ (M=Ni,Zn), Ionics 21 (2015) 2511–2522, https://doi.org/10.1007/s11581-015-1439-6.
[5] S. Han, B. Zhang, T. Tong, Z. Yang, S. Pan, Four alkali metal molybdates with two types of Mo-O chains, $ABMo_3O_{10}$ (A = Li, B = Rb; A = Li, Na, K, B = Cs): synthesis, structure comparison and optical properties, New J. Chem. 42 (2018) 10879–10884, https://doi.org/10.1039/c8nj01893f.
[6] A. Sarapulova, D. Mikhailova, A. Senyshyn, H. Ehrenberg, Crystal structure and magnetic properties of Li,Cr-containing molybdates $Li_3Cr(MoO_4)_3$, $LiCr(MoO_4)_2$ and $Li_{1.8}Cr_{1.2}(MoO_4)_3$, J. Solid State Chem. 182 (2009) 3262–3268, https://doi.org/10.1016/j.jssc.2009.09.012.
[7] D. Logvinovich, A. Arakcheeva, P. Pattison, S. Eliseeva, P. Tome S, I. Marozau, G. Chapuis, Crystal structure and optical and magnetic properties of $Pr_2(MoO_4)_3$, Inorg. Chem. 49 (2010) 1587–1594, https://doi.org/10.1021/ic9019876.
[8] S.R.S. Prabaharan, A. Fauzi, M.S. Michael, K.M. Begam, New NASICON-type $Li_2Ni_2(MoO_4)_3$ as a positive electrode material for rechargeable lithium batteries, Solid State Ionics 171 (2004) 157–165, https://doi.org/10.1016/j.ssi.2004.05.001.
[9] (a) K. Begam, S. Selladurai, Synthesis and redox behavior of a new polyanion compound, $Li_2Co_2(MoO_4)_3$, as 4 V class positive electrode material for lithium batteries, Ionics 10 (2004) 77–83, https://doi.org/10.1007/BF02410310;
(b) Z.A. Solodovnikova, I.A. Gudkova, E.S. Zolotova, V.N. Yudin, S. Division, Homogenety regions of double molybdates in the Na_2MoO_4–$MgMoO_4$ system and structures, J. Solid State Chem. 54 (2013) 917–925, https://doi.org/10.1134/S0022476613050119.
[10] E. de O. Gomes, L. Gracia, A. Santiago, R.L. Tranquilin, F. Motta, R.A.C. Amoresi, E. Longo, M.R.D. Bomio, J. Andrés, Structure, electronic properties, morphology evolution, and photocatalytic activity in $PbMoO_4$ and $Pb_{1-2x}Ca_xSr_xMoO_4$ (x = 0.1, 0.2, 0.3, 0.4 and 0.5) solid solutions, Phys. Chem. Chem. Phys. 22 (2020) 25876–25891, https://doi.org/10.1039/d0cp04596a.
[11] R. Grissa, H. Martinez, V. Pelé, S. Cotte, B. Pecquenard, F. Le Cras, An X-ray photoelectron spectroscopy study of the electrochemical behaviour of iron molybdate thin films in lithium and sodium cells, J. Power Sources 342 (2017) 796–807, https://doi.org/10.1016/j.jpowsour.2016.12.117.
[12] G.M. Gurgel, L.X. Lovisa, L.M. Pereira, F.V. Motta, M.S. Li, E. Longo, C.A. Paskocimas, M.R.D. Bomio, Photoluminescence properties of (Eu, Tb, Tm) co-doped $PbMoO_4$ obtained by sonochemical synthesis, J. Alloys Compd. 700 (2017) 130–137, https://doi.org/10.1016/j.jallcom.2016.12.409.
[13] S.S. Hosseinpour-Mashkani, A. Sobhani-Nasab, Synthesis and characterization of rod-like $CaMoO_4$ nanostructure via free surfactant sonochemical route and its

photocatalytic application, J. Mater. Sci. Mater. Electron. 27 (2016) 4351–4355, https://doi.org/10.1007/s10854-016-4303-1.
[14] V.B. Mikhailik, H. Kraus, G. Miller, M.S. Mykhaylyk, D. Wahl, Luminescence of $CaWO_4$, $CaMoO_4$, and $ZnWO_4$ scintillating crystals under different excitations, J. Appl. Phys. 97 (2005), 083523, https://doi.org/10.1063/1.1872198.
[15] N. Faure, C. Borel, M. Couchaud, G. Basset, R. Templier, C. Wyon, Optical properties and laser performance of neodymium doped scheelites $CaWO_4$ and $NaGd(WO_4)_2$, Appl. Phys. B Laser Opt. 63 (1996) 593–598, https://doi.org/10.1007/BF01830998.
[16] S.F. Solodovnikov, Z.A. Solodovnikova, E.S. Zolotova, V.N. Yudin, O.A. Gulyaeva, Y.L. Tushinova, B.M. Kuchumov, Nonstoichiometry in the systems Na_2MoO_4-$MMoO_4$ (M = Co, Cd), crystal structures of $Na_{3.36}Co_{1.32}(MoO_4)_{(3)}$, $Na_{3.13}Mn_{1.43}(MoO_4)_{(3)}$ and $Na_{3.72}Cd_{1.14}(MoO_4)_{(3)}$, crystal chemistry, compositions and ionic conductivity of alluaudite-type double molybdates and tungstates, J. Solid State Chem. 253 (2017) 121–128, https://doi.org/10.1016/j.jssc.2017.05.031.
[17] L.V. Balsanova, B.G. Bazarov, Synthesis and electrical properties of triple molybdates, Russ. J. Appl. Chem. 81 (2008) 1293–1295, https://doi.org/10.1134/S1070427208070331.
[18] S.G. Dorzhieva, B.G. Bazarov, A.K. Subanakov, J.G. Bazarova, Crystal structure modeling, electrical and thermal characterization of triple molybdates $RbCrTi_{0.5}(MoO_4)_{(3)}$ (R = Fe, Cr), J. Solid State Chem. 199 (2013) 21–26, https://doi.org/10.1016/j.jssc.2012.11.023.
[19] N.M. Kozhevnikova, Synthesis and study of the variable-composition phase $Na_{1-x}Co_{1-x}Fe_{1+x}(MoO_4)_{(3)}$, $0 <= x <= 0.4$, with Nasicon structure, Russ. J. Appl. Chem. 83 (2010) 384–389, https://doi.org/10.1134/S1070427210030031.
[20] J.B. Goodenough, H.Y.-P. Hong, J.A. Kafalas, Fast Na^+-ion transport in skeleton structures, Mater. Res. Bull. 11 (1976) 203–220, https://doi.org/10.1016/0025-5408(76)90077-5.
[21] J.A. Ibers, G.W. Smith, Crystal structure of a sodium cobalt molybdate, Acta Crystallogr. 17 (1964) 190–197, https://doi.org/10.1107/S0365110X64000482.
[22] R. Nasri, R. Marzouki, S. Georges, S. Obbade, M.F. Zid, Synthesis, sintering, electrical properties, and sodium migration pathways of new lyonsite $Na_2Co_2(MoO_4)_3$, Turk, J. Chem. 42 (2018) 1251–1264, https://doi.org/10.3906/kim-1801-89.
[23] M. Alvarez-Vega, U. Amador, M.E. Arroyo-de Dompablo, Electrochemical study of $Li_3Fe(MoO_4)_{(3)}$ as positive electrode in lithium cells, J. Electrochem. Soc. 152 (2005) A1306–A1311, https://doi.org/10.1149/1.1925069.
[24] B. Mehdaoui, H. Bensaid, L. Bih, R. Moubah, M.A. Valente, A. El Bouari, Magnetic properties of disordered $Li_2Co_{2-x}Ni_x(MoO_4)_3$ ($0 \le x \le 2$) system with a lyonsite structure, J. Supercond. Nov. Magnetism 32 (2019) 3549–3555, 0.1007/s10948-019-5128-y.
[25] M. Zouaoui, I. Jendoubi, M.F. Zid, F. Mohamed, N.F. Bourguiba, Synthesis, crystal structure and physico-chemical investigations of a new lyonsite molybdate $Na_{0.24}Ti_{1.44}(MoO_4)_{(3)}$, J. Solid State Chem. 300 (2021) 122221, https://doi.org/10.1016/j.jssc.2021.122221.
[26] B.I. Lazoryak, V.A. Efremov, Phases of $Na_{2x}Zn_2Sc_{2(1-x)}(MoO_4)_3$, $Na_{2x}Cd_2Sc_{2(1-x)}(MoO_4)_3$, $Na_{2x}Mg_2Sc_{2(1-x)}(MoO_4)_3$ changed composition, Zh. Neorg. Khim. 32 (1987) 652–656.
[27] A.L. Buzlukov, N.I. Medvedeva, Y.V. Baklanova, A.V. Skachkov, A.A. Savina, I.E. Animitsa, T.A. Denisova, E.G. Khaikina, Sodium-ion diffusion in alluaudite $Na_5In(MoO_4)_{(4)}$, Solid State Ionics 351 (2020) 115328, https://doi.org/10.1016/j.ssi.2020.115328.
[28] A.A. Savina, S.F. Solodovnikov, D.A. Belov, Z.A. Solodovnikova, S.Y. Stefanovich, B.I. Lazoryak, E.G. Khaikina, New alluaudite-related triple molybdates $Na_{25}Cs_8R_5(MoO_4)_{24}$ (R = Sc, In): synthesis, crystal structures and properties, New, J. Chem. 41 (2017) 5450–5457, https://doi.org/10.1039/C7NJ00202E.
[29] I. Ennajeh, S. Georges, Y.B. Smida, A. Guesmi, M.F. Zida, H. Boughazala, Synthesis, crystal structure, sintering and electrical properties of a new alluaudite-like triple molybdate $K_{0.13}Na_{3.87}MgMo_3O_{12}$, RSC Adv. 5 (2015) 38918, https://doi.org/10.1039/c5ra02276b.
[30] N.I. Sorokin, Ionic conductivity of double sodium–scandium and cesium–zirconium molybdates, Phys. Solid State 51 (2009) 1128–1130, https://doi.org/10.1134/S1063783409060079.
[31] I.Yu Kotova, D.A. Belov, S.Yu Stefanovich, $Ag_{1-x}Mg_{1-x}R_{1+x}(MoO_4)_3$ Ag^+ conducting NASICON-like phases, where R = Al or Sc and $0 \le x \le 0.5$, Russ. J. Inorg. Chem. 56 (2011) 1189–1193, https://doi.org/10.1134/S0036023611080122.
[32] N.M. Kozhevnikova, Vibrational spectra and electrophysical properties of a NASICON phase of variable composition $Na_{1-x}Co_{1-x}Sc_{1+x}(MoO_4)_3$, $0 \le x \le 0.5$, Russ. J. Inorg. Chem. 59 (2014) 1060–1065, https://doi.org/10.1134/S0036023614080142.
[33] N.M. Kozhevnikova, Synthesis and characterization of a NASICON phase of variable composition $Na_{1-x}Ni_{1-x}Sc_{1+x}(MoO_4)_3$ ($0 \le x \le 0.5$), Russ. J. Inorg. Chem. 59 (2014) 1225–1230, https://doi.org/10.1134/S0036023614090113.
[34] N.M. Kozhevnikova, Synthesis and study of the variable-composition phase $Na_{1-x}Co_{1-x}Fe_{1+x}(MoO_4)_3$, $0 \le x \le 0.4$, with Nasicon structure, Russ. J. Inorg. Chem. 83 (2010) 384–389, https://doi.org/10.1134/S1070427210030031.
[35] N.M. Kozhevnikova, S.Yu Batueva, Vibrational spectra and electrophysical properties of $Li_{0.2}K_{0.8-y}Mg_{1-x}Sc(Lu)_{1+x}(MoO_4)_3$ ($0 \le x \le 0.5$; $0 \le y \le 0.3$) solid solutions with a NASICON structure, Russ. J. Inorg. Chem. 63 (2018) 764–769, https://doi.org/10.1134/S0036023618060165.
[36] V.G. Grossman, J.G. Bazarova, M.S. Molokeev, B.G. Bazarov, New triple molybdate $K_5ScHf(MoO_4)_6$: synthesis, properties, structure and phase equilibria in the M_2MoO_4–$Sc_2(MoO_4)_3$–$Hf(MoO_4)_2$ (M = Li, K) systems, J. Solid State Chem. 283 (2020) 121143, https://doi.org/10.1016/j.jssc.2019.121143.
[37] A.E. Sarapulova, B. Bazarov, T. Namsaraeva, S. Dorzhieva, J. Bazarova, V. Grossman, A. Bush, I. Antonyshyn, M. Schmidt, A.M.T. Bell, M. Knapp, H. Ehrenberg, J. Eckert, D. Mikhailova, Possible piezoelectric materials $CsMZr_{0.5}(MoO_4)_3$ (M = Al, Sc, V, Cr, Fe, Ga, In) and $CsCrTi_{0.5}(MoO_4)_3$: structure and physical properties, J. Phys. Chem. 118 (2014) 1763–1773, https://doi.org/10.1021/jp4077245.
[38] J.G. Bazarova, A.V. Logvinova, B.G. Bazarov, Y.L. Tushinova, S.G. Dorzhieva, J. Temuujin, Synthesis of new triple molybdates $K_5RZr(MoO_4)_6$ (R = Al, Cr, Fe, In, Sc) in the K_2MoO_4–$R_2(MoO_4)_3$–$Zr(MoO_4)_2$ systems, their structure and electrical properties, J. Alloys Compd. 741 (2018) 834–839, https://doi.org/10.1016/j.jallcom.2018.01.208.
[39] V.G. Grossman, B.G. Bazarov, J.G. Bazarova, $K_5InHf(MoO_4)_6$: a solid state conductor, IOP Conf. Ser. Earth Environ. Sci. 320 (2019), 012050.
[40] E.Yu Romanova, B.G. Bazarov, R.F. Klevtsova, L.A. Glinskaya, YuL. Tushinova, K.N. Fedorov, ZhG. Bazarova, Phase formation in the K_2MoO_4–$Lu_2(MoO_4)_3$–$Hf(MoO_4)_2$ system and the structural study of triple molybdate $K_5LuHf(MoO_4)_6$, Russ. J. Inorg. Chem. 52 (2007) 749–752, https://doi.org/10.1134/S0036023607050154.
[41] B.G. Bazarov, R.F. Klevtsova, O.D. Chimitova, L.A. Glinskaya, K.N. Fedorov, YuL. Tushinova, ZhG. Bazarova, Phase formation in the Rb_2MoO_4–$Er_2(MoO_4)_3$–$Hf(MoO_4)_2$ system and the crystal structure of new triple molybdate $Rb_5ErHf(MoO_4)_6$, Russ. J. Inorg. Chem. 51 (2006) 800–804, https://doi.org/10.1134/S0036023606050196.
[42] B.G. Bazarov, T.V. Namsaraeva, R.F. Klevtsova, A.G. Anshits, T.A. Vereshchagina, R.V. Kurbatov, L.A. Glinskaya, K.N. Fedorov, ZhG. Bazarova, Phase equilibrium in the Cs_2MoO_4– $Bi_2(MoO_4)_3$–$Zr(MoO_4)_2$ system and the crystal structure of new triple molybdate $Cs_5BiZr(MoO_4)_6$, Russ. J. Inorg. Chem. 53 (2008) 1484–1488, https://doi.org/10.1134/S0036023608090222.
[43] B.G. Bazarov, O.D. Chimitova, R.F. Klevtsova, YuL. Tushinova, L.A. Glinskaya, ZhG. Bazarova, Crystal structure of a new ternary molybdate in the Rb_2MoO_4–$Eu_2(MoO_4)_3$–$Hf(MoO_4)_2$ system, J. Struct. Chem. 49 (2008) 53–57, https://doi.org/10.1007/s10947-008-0008-5.
[44] O.D. Chimitova, B.G. Bazarov, K.N. Fedorov, ZhG. Bazarova, Electrical properties of triple molybdates $Rb_5LnHf(MoO_4)_6$, Russ. J. Appl. Chem. 81 (2008) 2043–2044.
[45] V.G. Grossman, B.G. Bazarov, R.F. Klevtsova, L.A. Glinskaya, ZhG. Bazarova, Phase equilibria in the Tl_2MoO_4–$Fe_2(MoO_4)_3$–$Hf(MoO_4)_2$ system and the crystal structure of ternary molybdate $Tl(FeHf_{0.5})(MoO_4)_3$, Russ. Chem. Bull. 61 (2012) 1546–1549, https://doi.org/10.1007/s11172-012-0202-7.
[46] N.E. Novikova, V.G. Grossman, B.G. Bazarov, I.A. Verin, A.P. Dudka, S.Yu Stefanovich, J.G. Bazarova, New $Tl_{4.86}Fe_{0.82}Hf_{1.18}(MoO_4)_6$ ternary molybdate: crystal structure and properties, Acta Crystallogr. Section B 76 (2020) 839–849, https://doi.org/10.1107/S2052520620010768.
[47] V.G. Grossman, J.G. Bazarova, M.S. Molokeev, B.G. Bazarov, Thallium ionic conductivity of new thallium indium hafnium molybdate ceramics, Ionics 26 (2020) 6157–6165, https://doi.org/10.1007/s11581-020-03739-7.
[48] V.G. Grossman, S.V. Adichtchev, V.V. Atuchin, B.G. Bazarov, J.G. Bazarova, N. Kuratieva, A.S. Oreshonkov, N.V. Pervukhina, N.V. Surovtsev, Exploration of structural and vibrational properties of ternary molybdate $Tl_5BiHf(MoO_4)_6$ with isolated MoO_4 units and Tl^+ conductivity, Inorg. Chem. 59 (2020) 12681–12689, https://doi.org/10.1021/acs.inorgchem.0c01762.
[49] V.G. Grossman, M.S. Molokeev, B.G. Bazarov, J.G. Bazarova, Potassium and thallium conductors with a trigonal structure in the M_2MoO_4–$Cr_2(MoO_4)_3$–$Hf(MoO_4)_2$ (M = K, Tl) systems: synthesis, structure, and ionic conductivity, J. Alloys Compd. 873 (2021), https://doi.org/10.1016/j.jallcom.2021.159828, 159828.
[50] I. Madsen, R.J. Hill, Variable step-counting times for Rietveld analysis or getting the most out of your experiment time, Adv. X Ray Anal. 35 (1992) 39–47.
[51] I.C. Madsen, R.J. Hill, Collection and analysis of powder diffraction data with near-constant counting statistics, J. Appl. Crystallogr. 27 (1994) 385–392.
[52] Bruker AXS TOPAS V4: General Profile and Structure Analysis Software for Powder Diffraction Data. – User's Manual, Bruker AXS, Karlsruhe, Germany, 2008.
[53] B.G. Bazarov, T.T. Bazarova, K.N. Fedorov, Z.G. Bazarova, R.F. Klevtsova, L.A. Glinskaya, Synthesis and crystal structure of triple molybdate $K_5InHf(MoO_4)_6$, Zhurnal Neorganicheskoj Khimii 50 (2005) 1240–1243.
[54] C.E. Derrington, A. Linder, M. O'Keeffe, Ionic conductivity of some alkaline earth halides, J. Solid State Chem. 15 (1975) 171–174.
[55] V.G. Grossman, B.G. Bazarov, K.N. Fedorov, ZhG. Bazarova, Electrical properties of ternary molybdates, Russ. J. Appl. Chem. 83 (2010) 1074–1076.
[56] R.D. Shannon, Revised effective ionic radii and systematic studies of interatomic distances in halides and chalcogenides, Acta Crystallogr. A. 32 (1976) 751–767.